Evolution of nonconformal Landau-Levich-Bretherton films of partially wetting liquids

Michiel T. Kreutzer[*] and Maulik S. Shah
Department of Chemical Engineering, Delft University of Technology,
Van der Maasweg 9, 2629 HZ Delft, The Netherlands

Pravien Parthiban and Saif A. Khan[†]
Department of Chemical and Biomolecular Engineering, National University of Singapore,
Blk E5, 4 Engineering Drive 4, Singapore 117576

We experimentally and theoretically describe the dynamics of evolution and eventual rupture of Landau-Levich-Bretherton films of partially wetting liquids in microchannels in terms of nonplanar interface curvatures and disjoining pressure. While both the early-stage dynamics of film evolution and near-collapse dynamics of rupture are understood, we match these regimes and find theoretically that the dimensionless rupture time, T_r, scales with $\kappa^{-10/7}$. Here, κ is the dimensionless curvature given by the ratio of the Laplace-pressure discontinuity that initiates film thinning to the initial strength of the disjoining pressure that drives the rupture. We experimentally verify the rupture times and highlight the crucial consequences of early film rupture in digital microfluidic contexts: pressure drop in segmented flow and isolation of droplets from the walls.

I. INTRODUCTION

Rain droplets running on windows or over the surface of leaves are everyday examples of the delicate interplay of forced wetting, stability, and dewetting of thin liquid films deposited on repelling surfaces. A crucial question is whether a film of uniform thickness can coat the repelling surface without any gradients in film curvature. Such *conformal* films are found on flat plates, cylinders, and spheres, and, even on such simple surfaces, interesting transitions between coating and nonwetting states emerge with rich dynamics and transitions that typically involve careful analysis of the contact line and stability analysis involving perturbations of both the contact lineshape and film curvature [1]. The general physics of what happens to coating conformal thin films is now well understood. Briefly, for flat plates or cylindrical objects that are withdrawn at sufficient speed from a liquid bath, the Landau-Levich-Bretherton (LLB) theory [2] teaches that conformal films are pulled along. The deposited film thickness then scales as $h \sim \mathscr{C}^{2/3}$, where the capillary number $\mathscr{C} = \mu U/\gamma$, with viscosity μ, velocity U, and surface tension γ, signifies the ratio of viscous stress ($\sim \mu U/h$) to capillary pressure ($\sim \gamma/h$). The eventual fate of these wetting films, on partially wetting surfaces, is to form droplets. Small perturbations of film thickness grow and lead to rupture of the film and dewetting to droplets, with a dramatic height dependence of rupture time, $t \sim h^5$, such that a 1-μm film ruptures in 1 week and a 1-nm film ruptures in a second [3]. In contrast, on nonflat surfaces, e.g., near acute corners, in channels with rectangular cross sections or on topographically pre-patterned

---
[*]m.t.kreutzer@tudelft.nl
[†]chesakk@nus.edu.sg

014203-1

surfaces, even the static case without external flow is attended by polymorphism and topological bifurcations [4]. If, in addition, flow deposits nonconformal films, then sharp localized curvature gradients cause fluid flow and even in a fully wetting context profoundly influence the final shape of the deposited film [5,6]. Nonconformal partially wetting films exhibit accelerated film thinning and rupture with dramatic consequences: whereas moving elongated bubbles or drops in circular microchannels are surrounded by long-lasting thin films of the carrier liquid on the confining walls, in square channels such a well-behaved scenario is not observed for partially wetting fluids. In contrast, the flow is characterized by chaotic dynamics that are poorly understood [7].

In this paper, we address the open question of predicting the rupture time from a well-defined initial film shape, by studying a representative problem of confined long bubbles flowing in channels of rectangular cross section, such that the distance from the nose of the bubble directly relates to lifetime of the film. While significant progress has been made in understanding the evolution of such films in various limiting cases [8], a comprehensive analysis that encompasses all the stages of film evolution, and which ultimately predicts the rupture time, is still lacking. Briefly, the early stages of thinning have been studied in the context of marginal soap pinching and ophthalmology [6,9], while the main features of the final collapse are also understood [10]. We analyze the full dynamic evolution of such thin films, from deposition to thinning to rupture, with theoretical rupture times that can be compared to experiment. These rupture times find application beyond the time required to blink an eye to rewet it, as mentioned above. We highlight the consequences of partial wetting in the context of digital microfluidics, using the rupture time to delineate regimes with markedly different behavior.

II. EXPERIMENT

We recorded top-view micrographs of elongated bubbles coflowing with liquid [Fig. 1(a)] in a microchannel ($h_c \times w_c = 127 \times 300 \, \mu\text{m}^2$) that was manufactured using standard lithographic techniques such that all walls consisted of smooth polydimethylsiloxane (PDMS). Speed U and length l of monodisperse bubbles were independently varied by adjusting the gas and liquid feed rates into a T junction [11]. The channel was trans-illuminated by reflection from a white background and the microscope objective was focused on the bottom wall, such that droplets and film curvature were visible in high contrast [Fig. 1(b)]. The partially wetting liquid was ethanol (>99.9%) of viscosity $\eta = 1.09$ mPa s, surface tension $\gamma = 21.8$ mN/m, equilibrium contact angle $\theta_0 = 8°$ with air, and PDMS-ethanol-air Hamaker constant $A = 2 \times 10^{-21}$ J calculated from [12].

Flows at low speeds ($\mathscr{C} < 2.5 \times 10^{-5}$) showed no deposition of fluid on the wall [Fig. 1(c)]. This image clearly shows the contact line between the liquid in the corners of the channel (black) and the bare wall in the x-z plane. The z component of the velocity of this contact line is given by $U \cos \alpha$, where α is the angle of the normal of the contact line with the z axis, as shown in Fig. 1(e). Increasing the bubble speeds first resulted in a wetting film, first near the centerline of the channel where $\cos \alpha \approx 1$. This film is so thin that it immediately ruptures into the small droplets that are clearly visible in the image. Increasing the bubble velocity further increases the distance from the centerline where a film is deposited. Analysis of the data in Figs. 1(d)–1(g) revealed that the highest value of α for which a film was deposited was given by $\alpha \approx \cos^{-1}(\mathscr{C}_c/\mathscr{C})$ with the critical capillary number for the onset of forced wetting $\mathscr{C}_c \approx 3 \times 10^{-5}$, which is in reasonable agreement, assuming a slip length of 1 nm, with [13]. At even higher bubble speeds when $\alpha \sim \pi/2$, a film was deposited that spanned the entire cross section of the channel between the menisci at the sides [Figs. 1(h)–1(j)]. This film ruptured, always at the edge where the deposited film met the meniscus. We measured the distance z_r of unruptured film, as shown in Fig. 1(j) at five different locations on the microchip. With increasing $\mathscr{C}$, z_r increased from $z_r \approx 100 \, \mu\text{m}$ at $\mathscr{C} = 1.8 \times 10^{-4}$ to $z_r \approx 7.5$ mm at $\mathscr{C} = 2 \times 10^{-3}$, provided the bubble was long enough to observe any rupture at all. The standard deviation of the measurements at the five locations was 20–25 % for all experiments. At low speeds, the main source of uncertainty was the location of film deposition, i.e., the point where the curvature in the z direction has vanished, determined by fitting a circle and straight line to the inner black shadow of the micrographs [Fig. 1(i)]. At higher speeds, the main source of uncertainty
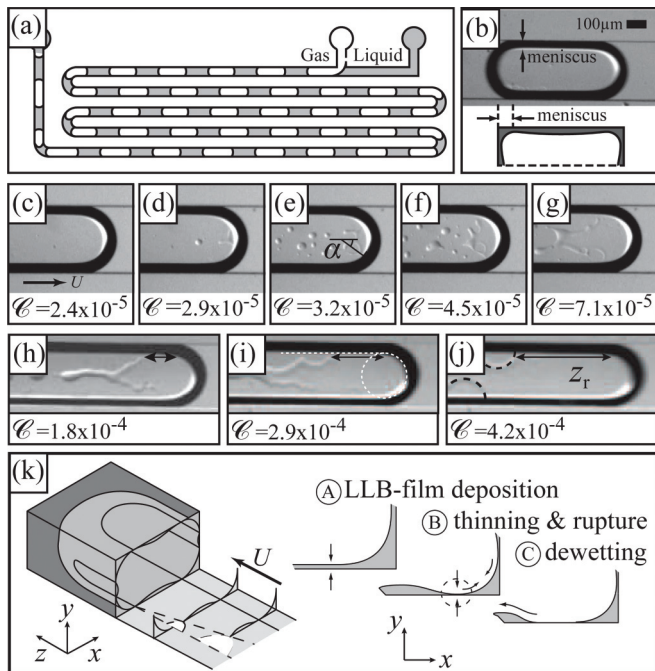
FIG. 1. (a) Sketch of the experimental setup. (b) Top-view micrograph of a flowing bubble; dark regions in the image indicate corner menisci. (c)–(g) Microscope observations of Landau-Levich-Bretherton (LLB) film deposition dynamics; films are deposited at capillary numbers $\mathscr{C} > 2.5 \times 10^{-5}$. (h)–(j) Observations of dewetting dynamics: films rupture at the corners and move along circular fronts; z_r is a speed-dependent length of unruptured film. (k) Schematic three-dimensional cutout near the nose of the bubble (left) and x-y cross sections of the lubricating film at increasing distance from the nose, depicting the important events, including film deposition, rupture, and dewetting (right).

was the interpolation between two frames to find the moment of rupture. We did this interpolation as follows: After rupture of the film near the meniscus, a dewetting front developed that spread out radially at 2.2 mm/s, independent of film thickness in agreement with theory [14]. We measured the radius of this front in several frames after rupture, as shown by the black dotted circles in Fig. 1(j). Then, we extrapolated the time evolution of this front to zero to achieve subframe resolution of the time and location of rupture. In turn, this subframe resolution of the rupture time straightforwardly allowed interpolation of the location of the nose at the rupture between two frames to find z_r.

The sequence of images in Figs. 1(c)–1(j) shows that there are three distinct regimes: a fully dewetted regime without a LLB film [Fig. 1(c)], a partially wetted regime where the LLB film ruptures, but such that the dewetting front cannot "catch up" with the nose [Figs. 1(d)–1(j)], and finally a fully wetted regime in which the lifetime of the LLB film is longer than the convective time l/U of the bubble. Jose and Cubaud [8] observed this last regime as a "lubricated" regime and observed droplets (bubbles) that at least partially wet the walls in the other two regimes. Their experimental data for different silicon oils with water droplets collapsed onto a regime boundary as $l/w = \zeta U^{1/3}\mathscr{C}^{2/3}$, where ζ is a dimensional constant. In the following, we derive this regime boundary from the evolution of the LLB film.

III. RUPTURE TIME FROM THIN-FILM EQUATION

A bubble moving through a rectangular microchannel, besides depositing thin films, also leaves liquid "gutters" along the channel edges, with a meniscus of radius $r^{-1} = (2w_c^{-1} + 2h_c^{-1})$ [Fig 1(b)].

Axial flow in these gutters can be ignored, but a Laplace pressure difference $p = \gamma/r$ causes transverse flow, which is balanced by viscous drag in the deposited film. Where the meniscus meets the flat part of the film, the film thins out by liquid drainage into a localized dimple, where long-range forces eventually induce a rapid collapse.

The evolution of the film thickness $h(x, t)$ in the dimple near the meniscus is described by the thin-film equation [1]

$$\partial_t h + \partial_x \left(\frac{\gamma}{3\mu} h^3 \partial_{xxx} h + \frac{A}{6\pi \mu h} \partial_x h \right) = 0 \tag{1}$$

in a region around $x = 0$ where the meniscus meets the thin film. We use the disjoining pressure approximation, in which the long-range intermolecular forces between the phases are replaced by a disjoining pressure $\Pi = A/6\pi h_0^3$ applied at the film boundary [15]. For negative x, the dimple region will match onto the stagnant meniscus of constant curvature, i.e.,

$$h = h_0 + \frac{x^2}{2r}, \quad \partial_{xx} h = r^{-1} \quad \text{for} \quad x \ll 0. \tag{2}$$

The film deposited by the nose is not flat and decreases in thickness from $h_0 \sim h_c \mathscr{C}^{2/3}$ near the centerline to $h_0 \sim h_c \mathscr{C}$ near the menisci at the sides, where h_c is the microchannel height [6]. Then, the initial slope and curvature for small and positive x are $\partial_x h \sim \mathscr{C}^{2/3}$ and $\partial_{xx} h \sim \mathscr{C}^{2/3}/w_c$, respectively, and for small $\mathscr{C}$ we may use

$$h = h_0, \quad \partial_x h = 0 \quad \text{for} \quad x \gg 0 \tag{3}$$

to complete the boundary conditions. Suitable choices of scales for time, transverse coordinate, and height are

$$t^* = \frac{12\pi^2 \mu \gamma h_0^5}{A^2}, \quad x^* = h_0^2 \sqrt{2\pi \gamma/A}, \quad h^* = h_0. \tag{4}$$

Scaling with $H = h/h^*$, $T = t/t^*$, and $X = x/x^*$ removes all parameters from Eq. (1) to get

$$\partial_T H + \partial_X \left(H^3 \partial_{XXX} H + \frac{1}{H} \partial_X H \right) = 0, \tag{5}$$

$$H = 1 + \tfrac{1}{2} \kappa X^2, \quad \partial_{XX} K = \kappa \quad \text{for} \quad X \ll 0, \text{and} \quad H = 1, \quad \partial_X H = 0 \quad \text{for} \quad X \gg 0 \tag{6}$$

and leaves only a dimensionless curvature

$$\kappa = \frac{\pi h_0^3 \gamma}{A} r^{-1} \tag{7}$$

in the boundary conditions. This last remaining parameter, κ, signifies the relative strength of the initial Laplace pressure jump (γ/r) at $x = 0$ to the disjoining pressure Π_0 at the initial film thickness.

Figure 2(a) shows a numerical solution of Eq. (1) for $\kappa = 50$, starting from $H = 1 + \kappa X^2$ $(x < 0)$, $H = 1$ $(x \geqslant 0)$. A depression in the film develops, having a minimum film thickness $H_{\min}$ near $x = 0$. First, a self-similar film profile develops, up to $H_{\min} \approx 0.2$ at $T = 2.3 \times 10^{-3}$, which marks the depth of the dimple region where long-range forces become prominent. From that moment onwards, the film thins out in a region $|X| < 0.1$, leading to rupture at $T = 2.5 \times 10^{-3}$. In this short time, the dimple profile is hardly affected outside the fast-pinching region, indicating how fast the final pinch is in comparison to the earlier thinning.

At early times, h is large and the dimple slope $\partial_x h$ is small, such that the disjoining pressure term in Eq. (1) may be ignored. Variables associated with this early stage are denoted by the symbol ˆ. Characteristic scales for time, height, and width of the dimple are

$$\hat{t}^* = \frac{3\mu r^4}{\gamma h_0^3}, \quad \hat{h}^* = h_0, \quad \hat{x}^* = \frac{x}{r}. \tag{8}$$
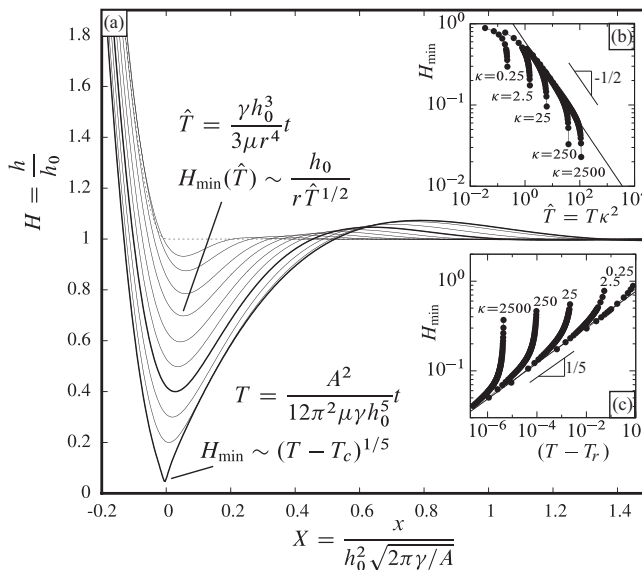
FIG. 2. (a) Dimensionless film height profiles H in the dimple region at various times $T = (0.01, 0.03, 0.08, 0.15, 0.27, 0.45, 0.75, 1.28, 2.0, 2.5) \times 10^{-3}$ from numerical solutions of Eq. (1) for $\kappa = 50$. The highlighted profile indicates a transition from an early drainage dominated regime [9] to a long-range force induced rupture regime [10]. (b), (c) Minimum film height $H_{\min}$ values extracted from numerical solutions of Eq. (1) for various κ are well described by the two self-similar expressions for minimum film height $H_{\min}$ provided in (a) at early and late times, respectively.

Now rescaling allows a self-similar solution [9], where the width of the dimple grows as $\hat{W} \sim h_0/r\hat{T}^{1/4}$ and the height of film decreases as $\hat{H}_{\min} \sim h_0/r\hat{T}^{1/2}$. Figure 2(b) shows that the evolution of the minimum in film thickness for $0.25 < \kappa < 2.5 \times 10^3$ all collapse onto a single master curve of $\hat{H}_{\min} \approx 0.6\hat{T}^{-1/2}$ of a monotonically decreasing thinning rate. This master curve describes the evolution of films that are still so thick that the disjoining pressure need not be taken into account. Films that are initially already so thin that the disjoining pressure is relevant from the start, such as that of $\kappa = 0.25$, never fully experience this regime. As soon as the long-range intermolecular term becomes dominant, however, the thinning rate increases, rapidly, as the early and late time scales are related as $\hat{T} = \kappa^2 T$: for large κ the time scale of the problem changes by orders of magnitude as the dimple moves through progressive stages of thinning. Close to the time of rupture, T_r, the evolution of the minimum film thickness is also amenable to a self-similar analysis [10], which predicts that $H_{\min} = 0.7681(T - T_r)^{1/5}$, independent of κ. We find indeed that for all κ, the final evolution of the minimum film height collapses onto this curve [Fig 2(c)]. Here too, note that for $\kappa = 0.25$, the film is initially so thin that its entire evolution collapses onto this curve.

We now explore whether we can match these two asymptotic descriptions to describe the entire evolution. The crudest matching is using the early curve for the minimal film height $H_{\min}$ up to a given H' at T' and then instantaneously switching to the other curve. This matching amounts to requiring that $H_{\min}$ and $\partial_T H_{\min}$ are continuous at T' and is, in fact, identical to calculating the value of H' for which the rupture is fastest, $\partial_{H'} T_r = 0$, as proposed by Vrij [16]. After some algebra, one finds that the crossover occurs at $T' = 0.913\kappa^{-10/7}$, with $H' = 0.627\kappa^{-2/7}$, and the film ruptures at $T_r = 1.278\kappa^{-10/7}$. Of course, when the film is initially so thin that rupture is dominated by van der Waals forces from the beginning, only the last asymptotic description is needed. One expects this to happen for $\kappa \ll 1$ and, indeed, we find $T_r = 13.0$ for all $\kappa < 0.196$. We find that this matching systematically overestimates the numerical rupture times, because at the crossover both capillary thinning and long-range forces are important. Following the structure of Eq. (1), in which
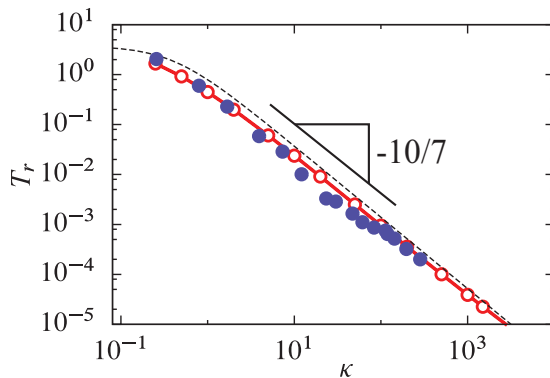
FIG. 3. Film rupture time versus dimensionless meniscus curvature κ. The red markers are numerical calculations. The dotted line is the theoretical prediction $T_r = 3.92[1 + 3.74\kappa^{10/7}]^{-1}$ obtained by matching the two self-similar solutions from Fig. 2. The blue markers represent experimental data of rupture times of ethanol films deposited around long bubbles on a PDMS surface.

the capillary term $\partial_X(H^3 \partial_{XXX} H)$ and long-range term $\partial_X(H^{-1} \partial_X H)$ contribute additively to the rate of thinning $\partial_T H$, it is better to add the thinning rates of both regimes. We begin by rewriting the rate of thinning, $\partial_T H$, in terms of H. For the early regime with $\partial_T H = -0.3\kappa^2(\kappa^2 T)^{-3/2}$ we use the $H = 0.6(\kappa T)^{-1/2}$ to eliminate T, to obtain $\partial_T H = -1.388\kappa^2 H^3$. Likewise for the late regime, we recast $\partial_T H = -0.1536(T_r - T)^{-4/5}$ into $\partial_T H = -0.053H^{-4}$. We then add these contributions to obtain the overall $\partial_T H$ and integrate the resulting $\partial_H T = (\partial_T H)^{-1}$ from initial to final height to obtain the rupture time. The rupture time is then given by

$$T_r = \int_0^1 (1.38\kappa^2 H^3 + 0.053H^{-4})^{-1} \, dH \approx 3.92[1 + 3.74\kappa^{10/7}]^{-1}. \tag{9}$$

The integral can be evaluated analytically to an impractically long expression, and the approximate solution is compact and captures the relevant physics, as it is based on the limiting values $T_r \to 3.92$ for $\kappa \to 0$ and $T_r \to 1.048\kappa^{-10/7}$ for $\kappa \to \infty$ of the full analytical solution. Figure 3 shows how well this prediction of rupture time agrees with the numerical simulations. For large κ, the analytical result tends to the numerical value. As can be seen in Fig. 2(b), for $\kappa \gg 1$ the two thinning regimes are well separated and the evolution of $H_{\min}$ runs closely along the asymptotic master curves. For smaller values of κ, the separation of the regimes is less pronounced and $H_{\min}$ does not evolve on the capillary master curve, which accounts for the small difference in analytical and numerical results. Nevertheless, the matching of the two regimes does identify the proper scaling of the rupture time with the only parameter of the problem, and the numerical results corroborate the $-10/7$ exponent derived above.

Returning to our experiments, we could easily vary the deposited film thickness by adjusting the bubble speed, with negligible impact on the meniscus curvature. We measured the time of rupture accurately as $t_r = z_r/U$. With experimental capillary numbers in the range $10^{-4} < \mathscr{C} < 3 \times 10^{-3}$, we used $h_0 \approx 0.5h_c\mathscr{C}$ [6] to estimate the initial film thickness in the range $h_0 \in [6–180]$ nm, such that our experiments spanned three orders of magnitude of κ and four decades of rupture time, $T_r = t_r/t^* = (8z_r A^2)/(3\pi^2 \gamma^2 h_c^5 Ca^6)$. Figure 3 shows that the time needed to rupture elongated bubbles in microchannels agrees very well with theory. In dimensional quantities, the large-κ limit of the rupture length, as measured from the nose of the bubble, is given by

$$z_r = 1.73\left(\frac{h_c^3 w_c^2}{(h_c + w_c)^2}\right)^{5/7} \left(\frac{\mu^3 U^3}{A\gamma^2}\right)^{4/7}, \tag{10}$$
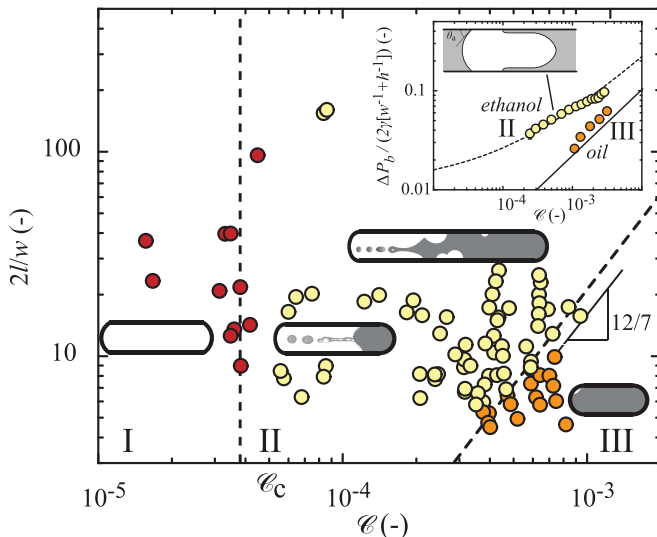
FIG. 4. Map of observed topological regimes, for PDMS-ethanol-air, arising from the dynamics of film deposition and rupture: (I) no film deposition below a threshold $\mathscr{C}$, (II) simultaneous film deposition and dewetting (a speed-dependent unruptured length of film exists in all cases), and (III) completely lubricated bubbles encapsulated in intact thin films. Inset: Measured pressure drop across bubbles depends strongly on the topological regime.

where for clarity we have isolated the geometric parameters from the flow parameters. The distance from the nose where dewetted patches of the lubricating film begin to grow is proportional to $U^{12/7}$, which is larger than the linear scaling $z_r \propto U$ that Jose and Cubaud [8] found. In our analysis, the time needed to rupture, t_r, increases with initial film thickness, which requires that $z_r = U t_r$ increases more than linearly with velocity.

IV. FLOW REGIMES AND PRESSURE DROP

In the context of digital microfluidics, droplets contain analytes and reagents that should remain isolated from each other and have no interaction, chemical or otherwise, with the wall. We consolidate our experimental observations in a topological map of dimensionless bubble length versus capillary number (Fig. 4), featuring two boundaries. The first, corresponding to a critical capillary number $\mathscr{C}_c \sim 3 \times 10^{-5}$, indicates the minimum speed to observe films at all. The second boundary shows how short the bubble must be to ensure complete surrounding by wetting films. This boundary is well predicted by our analysis of rupture times (Fig. 3) with $z_r \sim \mathscr{C}^{12/7}$ as shown in Fig. 4. The preceding analysis neglects the fluid above the lubricating film in the fluid-mechanical problem, which is appropriate for the bubbles we analyzed experimentally. For liquid droplets, however, this may not be the case, and effects on Hamaker constant and viscous drag need to be accounted for. However, we note that the latter effect may not be dominant, especially when droplet viscosity is lower than that of the carrier fluid, as is typically the case in microfluidic experiments.

To highlight the importance of partial wetting for the overall fluid mechanics of digital microflows, even at small contact angles, we now examine the implications of differences in film topologies on the frictional drag of bubble motion. We calculate the friction experienced by a flowing bubble, expressed as the pressure jump across the bubble, as $\Delta p_{\mathrm{B}} = (\Delta p - R U w h)/n$, where n is the total number of bubbles in the device. The hydrodynamic resistance, R, in the liquid segments is equivalent to flow without bubbles and given by $R = \eta [12/(1 - 0.63\, h w^{-1})](L_{\mathrm{liq}}/h^3 w)$. In experiments using fully wetting silicone oil ($\eta = 10$ mPa s, $\gamma = 20.1$ mN/m, $\theta_0 = 0°$) at $\mathscr{C} = O(10^{-3})$, we find indeed

that the pressure jump per bubble is a few percent of (γ/r) and scales as predicted, finding $\Delta p = 2.1\mathscr{C}^{2/3}(\gamma/r)$ within 25% of the theoretical value [6,17]. In the second regime in Fig. 4, the front of the bubble is lubricated by a wetting film that ruptures, and the rear is an advancing contact line. In this case, the net pressure jump over the bubble can be written in terms of curvature differences ΔC as $\Delta p_{\rm B} \sim \gamma \Delta C$. The curvature at the (lubricated) nose is $r^{-1}\cos\theta_e + \beta\mathscr{C}^{2/3}$ [6], and that at the rear can be written as $r^{-1}\cos\theta_a$ in terms of an advancing dynamic contact angle $\theta_a^3 = \theta_e^3 + 9\ln(r/\ell_m)\mathscr{C}$, where ℓ_m is a microscopic slip length [18]. In the inset of Fig. 4, we calculate the pressure drop for the partially lubricated bubbles. Interestingly, for $\mathscr{C} > 10^{-3}$, the pressure drop scales again as $\Delta p_{\rm B} \sim \mathscr{C}^{2/3}$ (which follows from expanding $1 - \cos\mathscr{C}^{1/3} \approx \frac{1}{2}\mathscr{C}^{2/3}$), but the pressure drop per bubble is a factor of 2 to 3 higher, even at the small contact angle $\theta_e = 8°$ of ethanol on PDMS. Recent experiments of pressure drop of bubbles in rectangular PDMS channels [19] did obey the $\Delta p \sim \mathscr{C}^{2/3}$ scaling, but also exhibited higher proportionality constants for aqueous surfactant solutions than those predicted by theory [6], which may well have been caused by partial wetting with small contact angles, in agreement with our experiments.

V. CONCLUSIONS

In conclusion, in this paper we explain the full evolution of nonconformal thin films under the action of surface tension and intermolecular forces. These nonconformal films exhibit LLB flat films connected to gutters that are akin to Plateau borders. The films first thin out due to capillary suction at the boundary between gutter and flat film to create a dimple, until intermolecular forces take over to rapidly thin out this dimple. The ratio of capillary and intermolecular forces, as expressed in a dimensionless parameter κ, determines how much of the thinning occurs in the first regime and how much in the second. We predict and experimentally verify the dimensionless moment of rupture as $T_r \sim \kappa^{-10/7}$. The present analysis offers a glimpse into the phenomena that mark the transition from regular droplet and pearl-type flows to chaotic flows in partially wetting channels [7,8].

[1] A. Oron, S. H. Davis, and S. G. Bankoff, Long-scale evolution of thin liquid films, Rev. Mod. Phys. **69**, 931 (1997); D. Bonn, J. Eggers, J. Indekeu, J. Meunier, and E. Rolley, Wetting and spreading, *ibid.* **81**, 739 (2009); J. H. Snoeijer and B. Andreotti, Moving contact lines: Scales, regimes and dynamical transitions, Annu. Rev. Fluid Mech. **45**, 269 (2013); P.-G. de Gennes, F. Brochard-Wyart, and D. Quéré, *Capillary and Wetting Phenomena: Bubbles, Pearls, Waves* (Springer, New York, 2004); P. G. de Gennes, Wetting—statics and dynamics, Rev. Mod. Phys. **57**, 827 (1985); J. Ziegler, J. H. Snoeijer, and J. Eggers, Film transitions of receding contact lines, Eur. Phys. J. Spec. Top. **166**, 177 (2009); M. Galvagno, D. Tseluiko, H. Lopez, and U. Thiele, Continuous and Discontinuous Dynamic Unbinding Transitions in Drawn Film Flow, Phys. Rev. Lett. **112**, 137803 (2014); J. H. Snoeijer, B. Andreotti, G. Delon, and M. Fermigier, Relaxation of a dewetting contact line. Part 1. A full-scale hydrodynamic calculation, J. Fluid Mech. **579**, 63 (2007).

[2] L. Landau and B. Levich, Dragging of a liquid by a moving plate, Acta Physicochim. URSS **17**, 42 (1942); F. P. Bretherton, The motion of long bubbles in tubes, J. Fluid Mech. **10**, 166 (1961); D. Quere, J. M. Dimeglio, and F. Brochard-Wyart, Spreading of liquids on highly curved surfaces, Science **249**, 1256 (1990); H. A. Stone, Batchelor prize lecture interfaces: In fluid mechanics and across disciplines, J. Fluid Mech. **645**, 1 (2010).

[3] A. Vrij and J. T. G. Overbeek, Rupture of thin liquid films due to spontaneous fluctuations in thickness, J. Am. Chem. Soc. **90**, 3074 (1968).

[4] R. Seemann, M. Brinkmann, E. J. Kramer, F. F. Lange, and R. Lipowsky, Wetting morphologies at microstructured surfaces, Proc. Natl. Acad. Sci. USA **102**, 1848 (2005); R. Mukherjee, D. Bandyopadhyay, and A. Sharma, Control of morphology in pattern directed dewetting of thin polymer films, Soft Matter **4**, 2086 (2008); S. Herminghaus, M. Brinkmann, and R. Seemann, Wetting and dewetting of complex surface geometries, Annu. Rev. Mater. Res. **38**, 101 (2008).

[5] A. De Lozar, A. Juel, and A. L. Hazel, The steady propagation of an air finger into a rectangular tube, J. Fluid Mech. **614**, 173 (2008).

[6] H. Wong, C. J. Radke, and S. Morris, The motion of long bubbles in polygonal capillaries. 1. Thin films, J. Fluid Mech. **292**, 71 (1995); The motion of long bubbles in polygonal capillaries. 2. Drag, fluid pressure and fluid-flow, *ibid.* **292**, 95 (1995).

[7] R. Dreyfus, P. Tabeling, and H. Willaime, Ordered and Disordered Patterns in Two-Phase Flows in Microchannels, Phys. Rev. Lett. **90**, 144505 (2003).

[8] B. M. Jose and T. Cubaud, Formation and dynamics of partially wetting droplets in square microchannels, RSC Adv. **4**, 14962 (2014).

[9] A. Aradian, E. Raphael, and P. G. de Gennes, Marginal pinching in soap films, Europhys. Lett. **55**, 834 (2001).

[10] W. W. Zhang and J. R. Lister, Similarity solutions for van der Waals rupture of a thin film on a solid substrate, Phys. Fluids **11**, 2454 (1999).

[11] P. Garstecki, M. J. Fuerstman, H. A. Stone, and G. M. Whitesides, Formation of droplets and bubbles in a microfluidic T-junction—scaling and mechanism of break-up, Lab Chip **6**, 437 (2006); V. van Steijn, C. R. Kleijn, and M. T. Kreutzer, Flows Around Confined Bubbles and Their Importance in Triggering Pinch-Off, Phys. Rev. Lett. **103**, 214501 (2009).

[12] J. Léopoldès and P. Damman, From a two-dimensional chemical pattern to a three-dimensional topology through selective inversion of a liquid-liquid bilayer, Nat. Mater. **5**, 957 (2006).

[13] T. Shing Chan, T. Gueudré, and J. H. Snoeijer, Maximum speed of dewetting on a fiber, Phys. Fluids **23**, 112103 (2011).

[14] C. Redon, F. Brochard-Wyart, and F. Rondelez, Dynamics of Dewetting, Phys. Rev. Lett. **66**, 715 (1991).

[15] B. Dai, L. G. Leal, and A. Redondo, Disjoining pressure for nonuniform thin films, Phys. Rev. E **78**, 061602 (2008).

[16] A. Vrij, Possible mechanism for the spontaneous rupture of thin, free liquid films, Discuss. Faraday Soc. **42**, 23 (1966).

[17] A. L. Hazel and M. Heil, The steady propagation of a semi-infinite bubble into a tube of elliptical or rectangular cross-section, J. Fluid Mech. **470**, 91 (2002).

[18] E. Rio, A. Daerr, B. Andreotti, and L. Limat, Boundary Conditions in the Vicinity of a Dynamic Contact Line: Experimental Investigation of Viscous Drops Sliding Down an Inclined Plane, Phys. Rev. Lett. **94**, 024503 (2005).

[19] M. J. Fuerstman, A. Lai, M. E. Thurlow, S. S. Shevkoplyas, H. A. Stone, and G. M. Whitesides, The pressure drop along rectangular microchannels containing bubbles, Lab Chip **7**, 1479 (2007).

[20] S. Khodaparast, O. Atasi, A. Deblais, B. Scheid, and H. A. Stone, Dewetting of thin liquid films surrounding air bubbles in microchannels, Langmuir (2018), doi: 10.1021/acs.langmuir.7b03839.